

Network-driven dispersion in transport phenomena

*Original*

Network-driven dispersion in transport phenomena / Vendruscolo, M., Salerno, L., Camporeale, C., Ridolfi, L.. - In: PHYSICAL REVIEW. E. - ISSN 2470-0045. - 111:5(2025). [10.1103/physreve.111.054313]

*Availability:*

This version is available at: 11583/3001849 since: 2025-07-16T07:29:38Z

*Publisher:*

American Physical Society

*Published*

DOI:10.1103/physreve.111.054313





*Terms of use:*


This article is made available under terms and conditions as specified in the corresponding bibliographic description in the repository

*Publisher copyright*

(Article begins on next page)

## Network-driven dispersion in transport phenomena

Margherita Vendruscolo <sup>\*</sup>, Luca Salerno , Carlo Camporeale , and Luca Ridolfi   
*Department of Environment, Land and Infrastructure Engineering (DIATI), Politecnico di Torino,  
 Corso Duca degli Abruzzi, 24, 10129 Torino, ITALY*

 (Received 9 October 2024; revised 13 February 2025; accepted 10 April 2025; published 22 May 2025)

A variety of key processes can be mathematically described in terms of directed transport networks, where a scalar (e.g., a signal or a substance) travels through a network until it reaches the exit. Different actions can intervene during transport, causing signal evolution. Here we focus on dispersion due to network connectivity. A mathematical model is built, under the hypothesis of exponential edge travel times. Three network elements are considered: network topology, edge-specific mean travel times, and signal partition at bifurcations. An analytical solution is given, which accounts for possible decay processes. Applications to model transport of conservative scalars in braided rivers and in random and small-world networks show the crucial role played by network-induced dispersion, the dominant role of edge travel times over bifurcation splitting rules, and occurrence of quasi-Gaussian shapes as the signal travels through the network.

DOI: [10.1103/PhysRevE.111.054313](https://doi.org/10.1103/PhysRevE.111.054313)

### I. INTRODUCTION

Networks are pervasive in natural, engineered, and social systems. Their description using appropriate mathematical tools is fundamental to explaining many phenomena around us [1–4]. In this area, which is experiencing great developments, we deal in particular with transport processes on directed networks.

Let us consider a graph composed of nodes interconnected by edges with given orientation, through which a scalar quantity (e.g., a signal, a chemical, etc.) is being transported. This quantity enters the network through the inlets, moves along the edges, and is distributed at the nodes according to application-specific rules. Finally, it leaves the network at the exit nodes. During transport, multiple processes may occur that influence output results, depending on the nature of the modeled phenomenon. In this work, we focus on dispersion induced by the network itself, explaining it in terms of network topology and edge-scale features, as schematically illustrated in Fig. 1.

We suppose purely advective transport, so that no dispersion occurs at the individual edges. If the network is composed of a unique path (i.e., a succession of single edges), then the insertion of any signal  $u(t)$  (a spike in Fig. 1) results only in temporal shifting of the same signal, without any shape modifications, as illustrated in the right panel of Fig. 1(a). Differently, if the signal is inputted in a more complex network, then the observed output consists of a different temporal distribution, as shown on the right in Fig. 1(b). This is due to

the presence of multiple heterogeneous paths, which the signal can follow from the inlet to the outlet. The output distribution is influenced by the length of the traveled edges and by how the signal splits when encountering bifurcations. In short, the network itself acts as a mixer on the input function, causing its time shape to change. We refer to this phenomenon as *network-induced dispersion*.

A beautiful natural example for this process, which triggered the present study, concerns transport processes in braided rivers (e.g., pollutants, seeds, sediments, large woods, pathogens). This class of rivers exhibits network-like morphologies, with multiple channels that split and merge continuously (see Fig. 2). It is easy to imagine that such complex topologies have a dispersive effect on any input distribution, in the sense indicated above.

It is important to keep in mind that network-induced dispersion may overlap with dispersive processes at the edge scale. For example, in networks that transport fluids (hydraulic networks, cardiovascular networks, etc.), the classic Taylor dispersion, due to the velocity profile in each edge [5], is present. However, mixing at the network scale induced by network topology, whose ingredients are the partition/joining in the nodes and the movement along the edges, remains unchanged.

In this work, we focus on this type of mixing by formulating a mathematical description of network-induced dispersion. To this aim, we draw inspiration from the theory of geomorphological dispersion (see [6–9]). This theory was developed to compute the hydrologic response of a river basin, while separating the contribution due to basin-scale river morphology from other mechanisms. Here we generalize the theory to the case of generic signal propagation through a network of any topology, by introducing a graph approach and relaxing river-related assumptions.

The mathematical model is based on a few hypotheses. We assume an exponential travel time distribution in each edge and transport through the network is modeled in the absence

<sup>\*</sup>Contact author: [margherita.vendruscolo@polito.it](mailto:margherita.vendruscolo@polito.it)

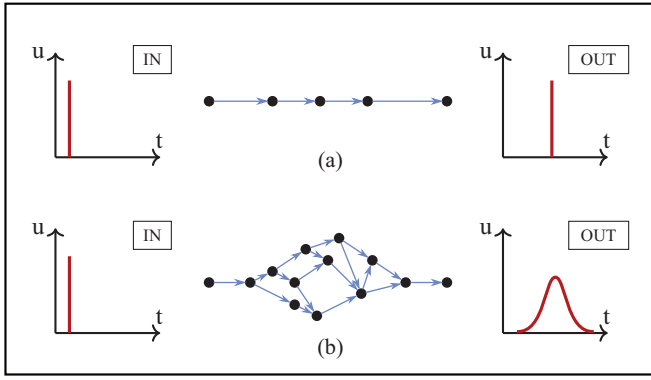


FIG. 1. Conceptual scheme for network-induced dispersion. The temporal behavior of signal  $u$  over time  $t$  is shown before and after traveling through the network (on the left and on the right, respectively). While in case (a) one observes only a temporal shifting of the signal, case (b) exhibits a dispersion component due to the network structure.

of storage at the nodes. In other words, this corresponds to transport out of one edge into the next ones until the exit is reached. Furthermore, the model assumes signal conservation, meaning that at the bifurcations the signal is split with no loss and at confluences contributions can be linearly summed. In Sec. IV we will discuss an extension to the case of decaying signals.

## II. MATHEMATICAL MODEL

Conceptually, our aim is to track a single particle as it moves in a directed single-inlet-single-outlet network. The particle is injected into the inlet at time  $t = 0$ , then follows a certain path to the outlet, where it stops. Each path is defined by a sequence of edges and has a certain probability of being chosen, depending on the splitting rules at bifurcations.

We want to determine the probability distribution of particle transit time throughout the network. In doing so, we consider the duration spent traveling in each edge and the probability of selecting a different path at every bifurcation.

We first derive the mathematical model to compute network-induced dispersion in a single-inlet-single-outlet case. The model is then extended to simulate dispersion in a network with multiple inlets and outlets.

The model is developed following the approach introduced in the seminal paper by Rodriguez-Iturbe and Valdés [6], who framed the problem of rainfall-runoff in a catchment as a semi-Markov process. The Markovian system is represented by a raindrop flowing through the river and the order of the stream at which the drop is located is the state that the system attains. Here, instead, we consider a particle moving through a generic network as the Markovian system and the edges are all possible states ( $i, j, k = 1, \dots, N$ , where  $N$  is the total number of edges in the network). The travel of the particle to the outlet, passing from edge to edge, is equivalent to transitions of the system from one state to another, up to the trapping state, i.e., the outlet edge. Furthermore, while in [6] the input consists of uniform instantaneous rainfall over the entire catchment, we consider a generic time-dependent distribution injected at specific edges (the inlets).

All graph edges exhibit different statistical features. For example, the waiting time that the particle spends in each edge before moving to the next one changes from edge to edge. Specifically, for edge  $i$ , the waiting time  $T_i$  is assumed to be an exponentially distributed random variable, with probability density function  $f_i(t) = \lambda_i e^{-\lambda_i t}$ , where  $\lambda_i$  is the inverse of the mean travel time in state  $i$ . We also define  $\bar{F}_i(t) = e^{-\lambda_i t} = \mathcal{P}[T_i > t]$  as the cumulative complementary distribution of  $T_i$ .

The transition between distinct edges is regulated by the transition probability matrix  $\mathbf{P}$ , whose each element denotes the likelihood of transitioning directly from one state to another. More specifically, if edge  $j$  is not contiguous to edge  $i$ , the component  $P_{ij}$  is assigned a value of 0. If  $j$  is the sole adjacent edge to  $i$ ,  $P_{ij}$  is set to 1. Finally, if  $i$  bifurcates into  $j$  and another edge  $k$ ,  $P_{ij}$  is a fractional value between 0 and 1 representing the probability to travel into  $j$  at the bifurcation, such that  $P_{ij} + P_{ik} = 1$ .

By using the above rules and definitions, [6] proposed that the probability  $\phi_{ij}(t)$  of traveling from any edge  $i$  to edge  $j$  within time  $t$  is regulated by the following equation:

$$\phi_{ij}(t) = \delta_{ij} \bar{F}_i(t) + \int_0^t \sum_{k=1}^N f_i(\tau) P_{ik} \phi_{kj}(t - \tau) d\tau. \quad (1)$$

The first term of Eq. (1), represents the probability of the particle remaining at edge  $i$  for longer than  $t$  (this term applies only when  $i = j$ ), while the second term is the probability of traveling from edge  $i$  to other edges  $k$  within a time period shorter than  $t$ , followed by a subsequent transition from  $k$  to  $j$  within the remaining duration. After defining two diagonal matrices  $\mathbf{f}$  and  $\bar{\mathbf{F}}$  such that

$$[\mathbf{f}(t)]_{ii} = f_i(t) \quad \text{and} \quad [\bar{\mathbf{F}}(t)]_{ii} = \bar{F}_i(t),$$

Eq. (1) can be expressed in matrix form as

$$\Phi(t) = \bar{\mathbf{F}}(t) + \int_0^t [\mathbf{f}(\tau) \mathbf{P}] \Phi(t - \tau) d\tau. \quad (2)$$

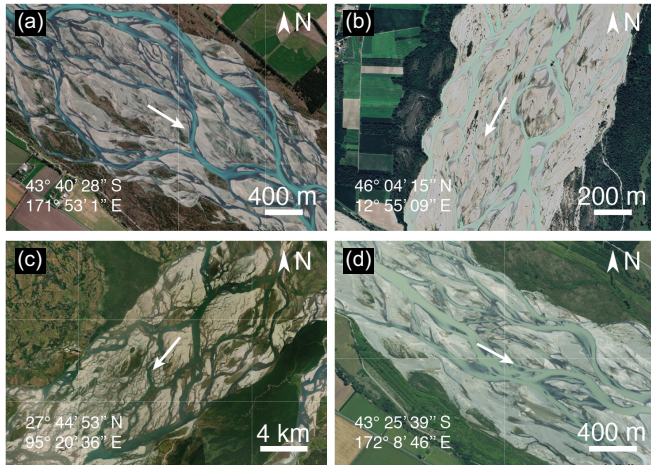


FIG. 2. Examples of networks of channels in braided rivers. The complex interaction between water flow and sediment supply generates these intricate networks of channels, separated by islands or sediment bars. The locations shown are (a) Rakaia River, New Zealand, (b) Tagliamento River, Italy, (c) Brahmaputra River, India, and (d) Waimakariri River, New Zealand. Water flow directions are indicated by the arrows. Coordinates refer to the center of each frame (coordinate reference system EPSG:4326 WGS 84).

The explicit solution for Eq. (2) can be obtained in the Laplace domain (see [10]), and after inverse transforming, one arrives to a solution for  $\Phi$  in the following exponential form

$$\Phi(t) = e^{\mathbf{A}t} = \mathbf{I} + \mathbf{A}t + \frac{\mathbf{A}^2 t^2}{2!} + \dots, \quad (3)$$

where  $\mathbf{A} = \mathbf{A}(\mathbf{P} - \mathbf{I})$  is the transition rate matrix and  $\mathbf{A}$  is a diagonal matrix containing the inverse mean waiting times  $\{\lambda_1, \lambda_2, \dots, \lambda_N\}$ . Component-wise, in Eq. (3) each matrix element

$$\phi_{ij}(t) = [e^{\mathbf{A}t}]_{i,j}$$

describes the probability of completing the travel between edge  $i$  and edge  $j$  within time period  $t$ .

We define  $\mathbf{X}$  as the  $N$ -dimensional row vector, whose elements  $X_j(t)$  represent the actual probability to occupy a edge  $j$  at time  $t$ . This depends on the initial condition for the particle, that is  $\mathbf{X}(0)$ . We have

$$\mathbf{X}(t) = \mathbf{X}(0)\Phi(t) \iff X_j(t) = \sum_{i=1}^N X_i(0)\phi_{ij}(t). \quad (4)$$

The initial conditions of the problem depend on the point of injection. In our case, the particle is injected into the inlet edge at time zero, meaning that only state  $in$  is occupied at time zero. This translates into the following definition for the initial condition:

$$X_i(0) = \begin{cases} 1 & \text{if } i = in, \\ 0 & \text{otherwise.} \end{cases} \quad (5)$$

To obtain the probability for a single particle to occupy the outlet at time  $t$ , we now select component  $j = out$  from Eq. (4). Then

$$X_{out}(t) = \sum_{i=1}^N X_i(0)[e^{\mathbf{A}t}]_{i,out} = [e^{\mathbf{A}t}]_{in,out}, \quad (6)$$

where in the second equivalence we used the definition of Eq. (5). Since  $out$  is the last (trapping) edge, Eq. (6) accounts for the probability that the particle has reached the outlet at time  $t$  or earlier.

In order to find the probability to exit the network at a specific time, we take the time derivative of Eq. (6), thus obtaining a probability density function

$$h(t) = \frac{d}{dt} X_{out}(t) = [\mathbf{A}e^{\mathbf{A}t}]_{in,out}. \quad (7)$$

More precisely,  $h(t)dt$  represents the probability that the particle reaches the outlet in the time interval  $[t, t + dt]$ . Considering the imposed initial conditions, this is equivalent to the network response to an impulse input distribution. Then, through convolution, Eq. (7) allows computation of the network output in response to any time-dependent distribution  $i_0(t)$  inputted at the inlet  $in$  as

$$\begin{aligned} u(t) &= \int_0^t h(t - \tau) i_0(\tau) d\tau \\ &= \int_0^t [\mathbf{A}e^{\mathbf{A}(t-\tau)}]_{in,out} i_0(\tau) d\tau. \end{aligned} \quad (8)$$

In cases with multiple inlets and outlets, the model is extended by linearly summing contributions from each inlet to the corresponding outlet, as explained in the following. Let us consider a network with  $N_{in}$  inlets and  $N_{out}$  outlets, indicated with subscripts  $in_i$  ( $i = 1, \dots, N_{in}$ ) and  $out_j$  ( $j = 1, \dots, N_{out}$ ). To determine the travel time distribution at the outlets, we first compute the impulse response function as in Eq. (7) for each inlet-outlet pair  $h_{in_i, out_j}(t)$ . Afterwards, each of these is convolved with the initial distribution  $i_{0,i}$  relative to  $in_i$  and summed over all inlets to find  $u_{out_j}(t)$ , that is the response at outlet  $out_j$  as a consequence of all different inputs:

$$u_{out_j}(t) = \sum_{i=1}^{N_{in}} \int_0^t h_{in_i, out_j}(t - \tau) i_{0,i}(\tau) d\tau. \quad (9)$$

For simplicity, when dealing with multiple outlets network, we can combine the distributions at the different outlets into a single function by summing them:

$$u(t) = \sum_{j=1}^{N_{out}} u_{out_j}(t). \quad (10)$$

Relations (8)–(10) therefore describe dispersion effect of a network, given (i) its topology (i.e., its adjacency matrix), (ii) the probability of partition between the outgoing edges in each of its nodes (i.e., matrix  $\mathbf{P}$ ), (iii) the mean traveling time for each edge (i.e., matrix  $\mathbf{A}$ ), and (iv) the temporal trends of the input signals [i.e., the  $i_0(t)$ ].

In the continuing of the paper, we present some illustrative examples derived from the model implementation, which investigate the influence of each model component (i)–(iv) on dispersion. In the next section, we show an application of the model to a fluvial network. Later in the Discussion, we will also consider some canonical network classes, such as random and small-world networks.

### III. EXAMPLE OF A BRAIDED RIVER NETWORK

The process we modeled in the previous section holds general validity for any case where a scalar is being transported through a network, under the hypothesis of exponential travel time distributions in each edge. Here we present an application to transport in a braided river. The reason for this choice lies in the fact that rivers constitute a quite intuitive example of networks paired with transport phenomena, and braided rivers exhibit naturally complex networks. In this case, the transported scalar may represent any conservative substance, e.g., a nonreactive chemical (pollutant or nutrient) or suspended particles (seeds or sediments).

We establish a correspondence between mathematical objects defined in the previous section and variables relative to fluvial transport, more specifically between the probability densities computed earlier and volume fractions of the transported substance. The input distribution  $i_0(t)$  represents the time-dependent injection of a certain volume of substance at the upstream inlet branches. This substance is assumed to be conservative, meaning that no mass losses occur during the downstream transport, so that the entire injected volume eventually reaches the outlet. Probability  $h(t)dt$  that the particle reaches the outlet at a certain time corresponds to the

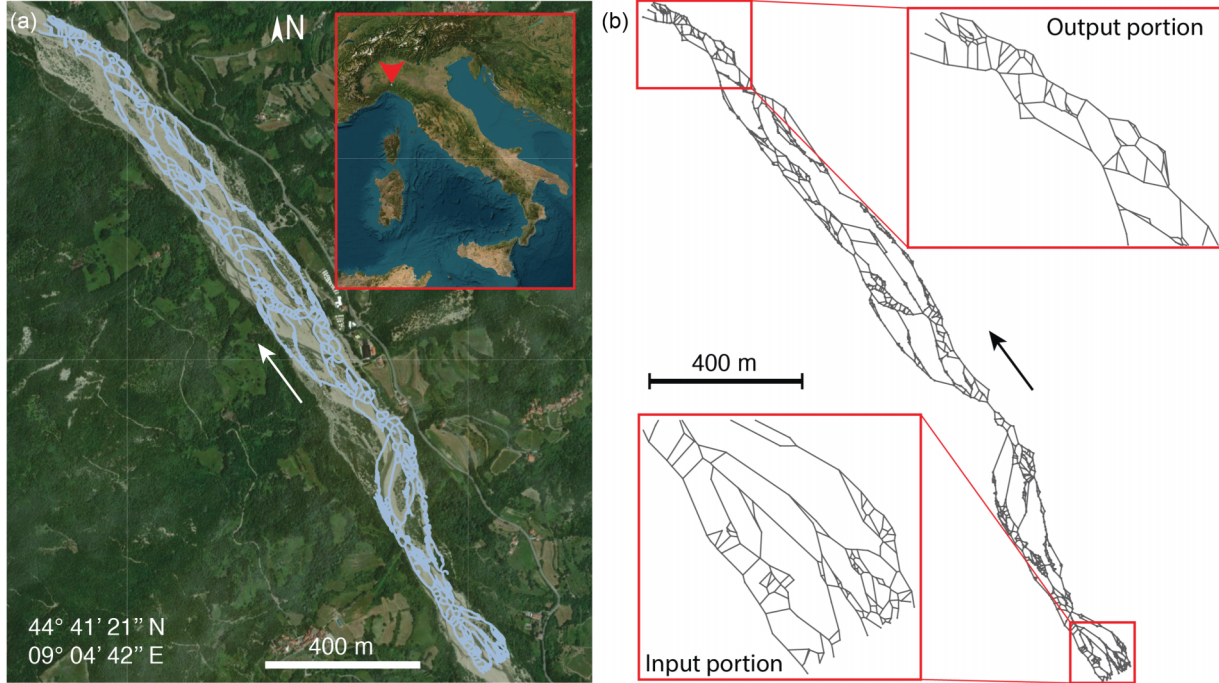


FIG. 3. River network of the Borbera River in northwestern Italy. (a) Polylines representing the channel centerlines derived from the wetted area results of the hydrodynamic numerical simulation. (b) Network topology extracted from the polylines, with a zoom-in on the input and output sections of the analyzed river reach. Water flow direction is indicated by the arrows. The coordinates refer to the center of the frame (coordinate reference system EPSG:4326 WGS 84).

substance volume fraction that arrives at the river outlet in the interval  $[t, t + dt]$  as a consequence of an instantaneous input injection. The network response  $u(t)$  represents the discharge distribution of the substance at the outlet, resulting from an input injection described by  $i_0(t)$ . Finally, each edge of the network corresponds to a river branch or channel, in which properties (slope, flow velocity, etc.) are considered uniform.

The fluvial example refers to the Borbera River, which flows in northwestern Italy [see Fig. 3(a)] and whose network is displayed in Fig. 3(b). Network topology is derived from results of previously performed hydrodynamic simulations of a 2.5 km river reach. The riverbed, which corresponds to the simulation domain, is reconstructed using remote sensing techniques, resulting in a digital terrain model. Multiple flow conditions are simulated, and for this study the condition with the highest number of active channels is selected. From the simulations, maps of wetted areas are extracted and simplified into polylines representing the centerlines of each channel. A GIS-based protocol [11] is adapted to convert the spatial polyline data into network formats. The network is then further refined to remove isolated branches. The network covers a river stretch of approximately 2500 m and is composed of 1248 nodes and 1746 edges, with 503 bifurcations. There are 15 inlets and five outlets, and no cycles exist. The water discharge in the network is assumed to be constant, equal to  $35 \text{ m}^3/\text{s}$  and divided evenly by the number of inlets. Water flow in all edges is obtained using a simplified set of equations involving branch slopes and inflow discharge. This procedure is based on basic hydraulic principles and is summarized in Appendix.

Model ingredients—bifurcation probability values  $P_{ij}$  and inverse mean travel times  $\lambda_i$  in each branch—are derived from the water flows. At each bifurcation the probabilities are obtained as the ratio between water flows  $Q_w$  in the outgoing and incoming branches. For example, if branch  $i$  splits into  $j$  and  $k$ , the values are computed as

$$P_{ij} = \frac{Q_{w,j}}{Q_{w,i}}, \quad P_{ik} = \frac{Q_{w,k}}{Q_{w,i}}. \quad (11)$$

Since  $Q_{w,i} = Q_{w,j} + Q_{w,k}$ , it is ensured that probabilities add up to one. The inverse branch mean travel times  $\lambda_i$  are estimated using branch-specific lengths and average flow velocities, which can be obtained from water flows as reported in the Appendix [see Eq. (A3)].

For the substance input signal we use a square function, defined so that the same dimensionless volumetric concentration of substance  $C_s = 0.01$  is imposed in each inlet for the entire injection time (hereinafter subscript "s" will always be used to mark variables relative to the substance). In particular in all inlets *in* the time-dependent discharge  $Q_{s,\text{in}}$  reads

$$Q_{s,\text{in}}(t) = \begin{cases} C_s Q_{w,\text{in}} & \text{if } 50 \text{ s} < t < 350 \text{ s,} \\ 0 & \text{otherwise.} \end{cases}$$

Note that, due to the assumption of linearity in the model, once the width of the square input is defined, results can be easily rescaled to accommodate different substance concentrations.

To study the evolution of substance discharges during transport, we select 12 cross sections (C-1, ..., C-12), spanning from upstream to downstream. The three upstream cross sections (C-1, C-2, and C-3) are placed at a closer distance

than the others to provide a detailed view of the process close to the injection point. Since each cross section typically intersects multiple edges, the signals computed in each of these edges are aggregated as in Eq. (10), in order to obtain a single representative discharge for each cross section. The results discussed below refer to these summed signals.

Results are presented as follows. First, we will consider a realistic fluvial case, model parameters (bifurcation probabilities and mean travel times) being obtained by the physically based procedure described above. Second, we will change mean travel times values and bifurcation probabilities, so as to highlight the impact of each component on the results.

Before moving on to the examples, we introduce the following metrics, that will be used for results interpretation. Let  $Q_s(t)$  represent the substance discharge at an outlet. We define the area under the curve as  $A_{Q_s} = \int_0^{t_{\max}} Q_s(t) dt$ , with  $t_{\max}$  being the last simulation time step. Note that  $A_{Q_s}$  represents the volume of substance flowing in the considered outlet. When summed over all outlets at each cross section, this value remains constant, equal to the total volume initially injected in the network. The following quantities are computed:

$$\begin{aligned}\mu_{Q_s} &= \frac{1}{A_{Q_s}} \int_0^{t_{\max}} t Q_s(t) dt, \\ \sigma_{Q_s} &= \sqrt{\frac{1}{A_{Q_s}} \int_0^{t_{\max}} (t - \mu_{Q_s})^2 Q_s(t) dt}, \\ Sk_{Q_s} &= \frac{1}{A_{Q_s}} \int_0^{t_{\max}} \left( \frac{t - \mu_{Q_s}}{\sigma_{Q_s}} \right)^3 Q_s(t) dt, \\ Ku_{Q_s} &= \frac{1}{A_{Q_s}} \int_0^{t_{\max}} \left( \frac{t - \mu_{Q_s}}{\sigma_{Q_s}} \right)^4 Q_s(t) dt.\end{aligned}$$

The mean value,  $\mu_{Q_s}$ , corresponds to the average time required for the substance to reach the outlet and approximately aligns with the peak time of  $Q_s(t)$ . Instead, the standard deviation  $\sigma_{Q_s}$  reflects the temporal spread of  $Q_s(t)$ , thereby quantifying dispersion.  $Sk_{Q_s}$  is the skewness of distribution  $Q_s(t)$  and measures its asymmetry. We recall that a skewness equal to zero is associated with a distribution that is symmetric around its mean, so that negative (positive) values correspond to a tail on the left (right) side of the distribution. Last,  $Ku_{Q_s}$ , called kurtosis, describes the tails of distribution  $Q_s(t)$ . Let us mention that a Gaussian distribution has  $Ku = 3$ , while kurtosis values larger than 3 indicate fatter tails.

A path from inlet to outlet is composed of a certain number of consecutive edges, whose waiting times are an exponentially distributed random variables. Therefore, we expect the travel time of a single path to have a hypo-exponential distribution, resulting from the convolution of exponential distributions [12]. Hypo-exponential distributions are often approximated by a Gaussian curve (see [13,14]); in particular if we assume all edge waiting times to be identically distributed we can refer to the classical Central Limit Theorem. Since the entire network travel time is a combination of the output coming from each path, it is therefore reasonable to compare the network outlet discharge  $Q_s(t)$  with Gaussian distributions. For this purpose, we define  $G_{Q_s}(t)$  as the corresponding Gaussian of

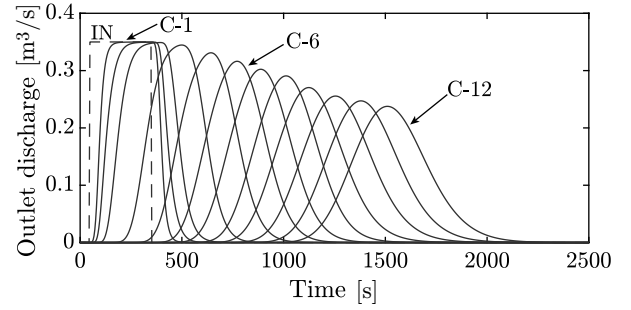


FIG. 4. Outlet discharges for the realistic fluvial case. The square input function curve is dashed and labeled “IN”. Each of the other curves represents the outlet discharge at a cross section C- $i$ , in order. For clarity, only the labels for cross sections C-1, C-6, and C-12 are indicated.

distribution  $Q_s(t)$ :

$$G_{Q_s}(t) = \mathcal{N}(\mu_{Q_s}, \sigma_{Q_s}^2) A_{Q_s}.$$

This is a normal distribution with the same mean value and standard deviation of  $Q_s(t)$  but an underlying area rescaled to  $A_{Q_s}$ ; it is therefore not a probability distribution, but it inherits the Gaussian shape. Finally, we introduce a metric to compute the distance between  $Q_s(t)$  and its corresponding Gaussian  $G_{Q_s}(t)$ . This is defined as

$$\|Q_s - G_{Q_s}\| = \frac{1}{t_{\max}} \sqrt{\int_0^{t_{\max}} [Q_s(t) - G_{Q_s}(t)]^2 dt}. \quad (12)$$

Dividing by  $t_{\max}$  allows the metric to have the same dimensions as  $Q_s(t)$ .

### A. Realistic case

In this section we simulate transport in the Borbera network, setting realistic values for the edges mean travel times and bifurcation probabilities. The input square function is distributed among the inlets and observed as it travels along the network.

Figure 4 shows a comparison between the squared input injection and the substance flows computed at each cross section along the network. The input is represented with a dashed line and labeled “IN”, while each of the outlet discharges in solid line refers to a transect of the network C- $i$  in order with  $i$  going from 1 to 12 (for simplicity only a few labels C- $i$  are indicated within the plot). As expected, the signal is shifting to the right in time, as the cross sections are positioned downstream in the direction of the water flow. Moreover, a noticeable smoothing and widening of the signal occurs, which is evidence of the dispersive nature of the transport process within the network. This key aspect is further explored by analyzing how mean, standard deviation, skewness and kurtosis change during the process, as displayed in Fig. 5. As a spatial “coordinate” for characterizing transport processes along the network, we use the number of bifurcations progressively encountered by substance while traveling downstream. This is obtained by counting the bifurcations in the network portion up to each cross section C- $i$ . A number of bifurcations equal to zero corresponds to the network inlet, therefore to

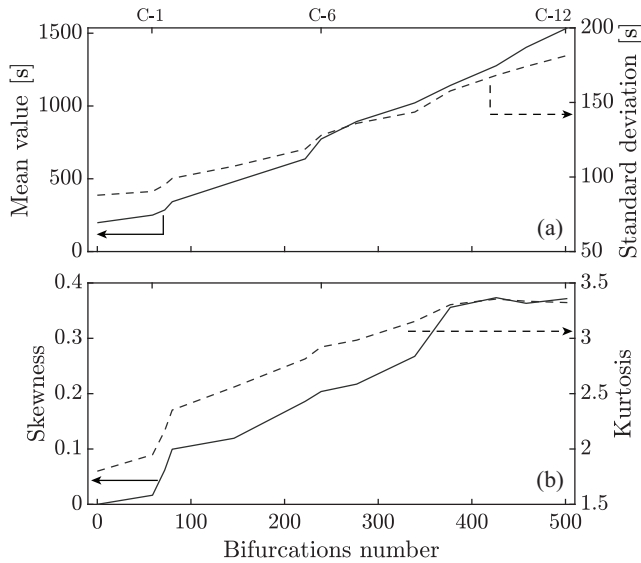


FIG. 5. Metrics relative to the outlet discharge for the realistic fluvial case. Panel (a) displays the mean value (solid line) and standard deviation (dashed line), and panel (b) the skewness (solid line) and kurtosis (dashed line) of the temporal behavior of the substance outlet discharges plotted over bifurcations number. Labels along the upper  $x$  axis indicate some cross sections in correspondence with their number of bifurcations. Continuous and dashed arrows indicate the corresponding  $y$  axes.

the initial square input distribution. We choose this coordinate because we expect the number of bifurcations to be directly related to the number of possible paths, and, as anticipated in the Introduction, paths heterogeneity plays a crucial role in determining dispersion of a transported signal. Figure 5(a) shows mean value and standard deviation of the substance discharge curves at each cross section. Both metrics increase with the number of bifurcations, i.e., during transport. This highlights the dispersion introduced by the network. Indeed, without dispersion one would only observe a translation of the signal on the time axis and an increase in the mean value with river length, while the standard deviation would remain unchanged.

Figure 5(b) reports the values of skewness and kurtosis of the substance discharges at the end of each network portion. We observe that both skewness and kurtosis increase with the number of bifurcations. This indicates that, as the signal travels downstream, its distribution becomes increasingly asymmetric, with a rightward tail, and its tail gradually thickens. Furthermore, we notice that, when the number of bifurcations reaches around 400, both skewness and kurtosis appear to stabilize. Specifically, skewness sets on a positive value, representing a permanent rightward asymmetry in the discharge curves, while kurtosis levels off at a value slightly above 3, which corresponds to that of a Gaussian curve.

### B. Impact of travel times and bifurcation probabilities

This section introduces some *ad hoc* modifications to the model parameters setting, aimed at investigating the influence of bifurcation probabilities and mean travel times.

Regarding bifurcations, we consider three cases overall: (i) realistic bifurcation probability values, like the ones used previously in Sec. III A, obtained as in Eq. (11), (ii) equal probabilities that substance travels from  $i$  to each of the two downstream branches  $j$  and  $k$ , i.e.,  $P_{ij} = P_{ik} = 0.5$  (at every bifurcation of  $i$  into  $j$  and  $k$ ), and (iii) random probability values, i.e.,  $P_{ij}$  and  $P_{ik}$ , extracted from a uniform distribution in the interval  $[0.1, 0.9]$  and satisfying the constraint  $P_{ij} + P_{ik} = 1$ .

Three cases are considered for edge mean travel times as well: (i) we use realistic mean travel times, like in Sec. III A, obtained using edge lengths and average velocities as shown in Eq. (A3), (ii) identical mean travel times are attributed to all the edges of the network, each equal to the average value of the realistic travel times (7.63 s), and (iii) edge-specific mean travel times are randomly extracted from a gamma distribution (which imitates the the distribution of realistic travel times) with shape parameter  $\alpha = 0.31$ , chosen to match skewness of the realistic travel times distribution, and a scale parameter  $\beta = 24.84$ , so that the mean remains around  $\alpha \beta \approx 7.7$  s.

To summarize, since both bifurcation probabilities and mean travel times can take either realistic, equal, or random values, there are nine possible parameter combinations, each representing a distinct case to be simulated and compared. Note that when dealing with random values, results are obtained by averaging the output of 30 realizations of the transport process in the network.

Finally, to investigate the long-term behavior of the system, we simulate the effect of a larger network by replicating the current network configuration. Specifically, we assume that once the substance discharge reaches the outlet, it is reinjected upstream, distributing it among the inlets, as a new input distribution. This allows us to follow the dispersion process for a longer time and is particularly useful to investigate the "stabilization" of skewness and kurtosis values which we observed in Fig. 5(b). The iteration process is repeated four times, therefore the final compound network is made up of 4992 nodes, 6984 edges, and 2012 bifurcations. We indicate by  $N_{it} = 1, \dots, 4$  the network iteration number.

Figure 6 displays the resulting outlet discharge curve for all nine cases after one, two, and four passages through the network ( $N_{it} = 1, 2$ , and 4). At first glance, one observes that the curves are grouped three by three according to their color, corresponding to the different methods used for selecting the mean travel times. In contrast, the different line styles are hardly visible due to overlap, meaning that changing the bifurcation probability values does not appear to have such a significant impact on the characteristics of the outlet discharge. This suggests that, compared to the other model component, edges travel time plays a dominant role in determining the main features of substance distributions at the outlet, particularly with regard to the mean value.

Looking at Fig. 6 it is interesting to observe that the substance reaches the outlet much earlier in the case where we use realistic travel times than the other cases. This is most likely due to how  $\lambda_i$  are distributed spatially. In fact, in the realistic cases edges with long travel times are typically distributed in parallel with multiple edges with shorter ones. This is not the case when travel times are assigned randomly, as it can result

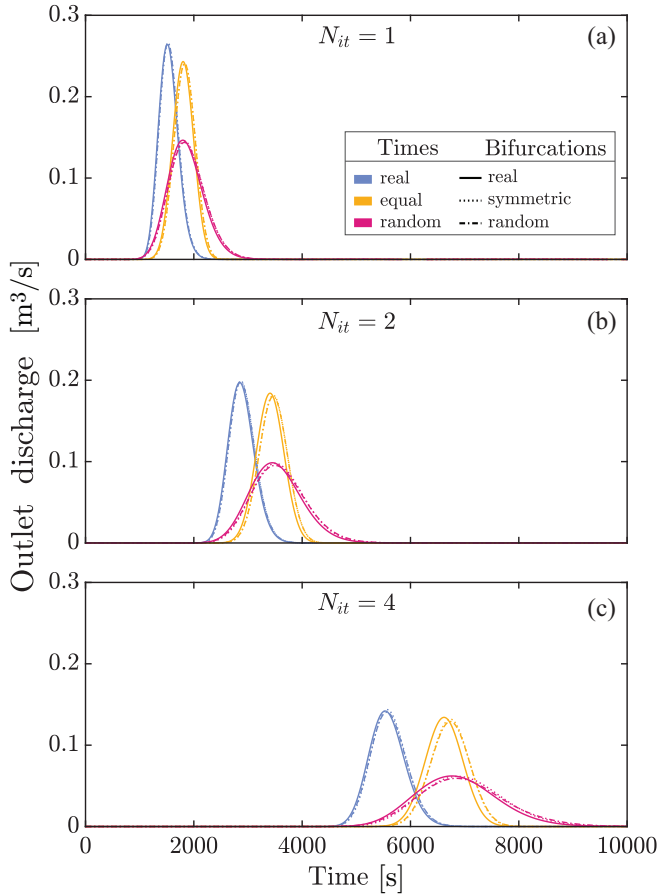


FIG. 6. Outlet discharges for nine simulation cases. Panel (a) shows the results after one network iteration, panel (b) after the two iterations, and panel (c) after four iterations. Different colors represent various choices for the edges mean time parameter, while the line styles indicate the type of bifurcation used, as reported in the legend. Notice that outlet discharges tend to be grouped according to the selected time parameter, to the point where curves of the same color overlap and the line style is hardly visible.

in several consecutive branches with long travel times. This (random) sequential arrangement significantly increases the time required for the substance to reach the outlet.

We observe that outlet discharges curves resemble Gaussian shapes, as expected. We investigate this similarity by using the metric defined in Eq. (12) to compute the distance between each signal and its corresponding Gaussian at the end of each network subsection. This allows us to track the evolution of these distances for all nine cases the network subsections, as shown in Fig. 7. The initial value on the  $x$  axis refers to the distance between the square input function and its corresponding Gaussian, which is identical for all cases. All the plotted curves exhibit a sharp decline when the bifurcations number fall in the interval  $[0, 300]$ , indicating that that a few bifurcations are sufficient to produce a strong dispersive effect. Beyond this point, the decrease continues, but at an increasingly slower rate. Notice that the yellow lines, corresponding to a choice of all equal mean edge travel times, exhibit values closer to zero compared to the other cases. We can ascribe this behavior to the already mentioned

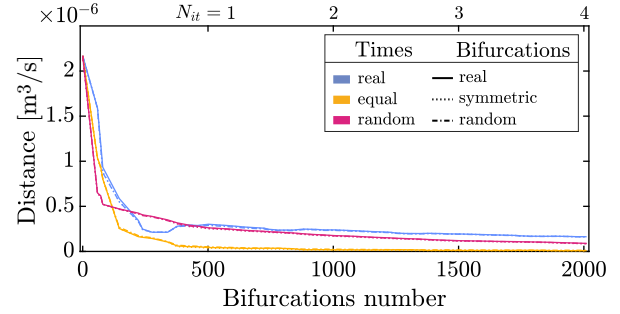


FIG. 7. Values of the distance between discharges  $Q_s$  and their respective Gaussians  $G_{Q_s}$ , computed as in Eq. (12), over the bifurcations number for all nine cases. Labels along the upper  $x$  axis indicate the exit of each network iteration in correspondence with its number of bifurcations. Different colors represent various choices for the edges mean time parameter, while the line styles indicate the type of bifurcation used, as reported in the legend. Lines with the same color tend to overlap due to the dominant role of the choice for mean travel times in the process.

Central Limit Theorem (see Sec. III); indeed, in this case all exponential distributions of the individual edges travel times are identical.

Figures 8 and 9 show metrics regarding the substance discharge curves plotted as functions of the number of bifurcations to investigate specific features of signal evolution along the transport process. In Fig. 8(a) mean values are shown. We can observe that blue lines (corresponding to cases with realistic edge travel times) always lie under other lines (i.e., cases with all equal and random mean travel times). In line

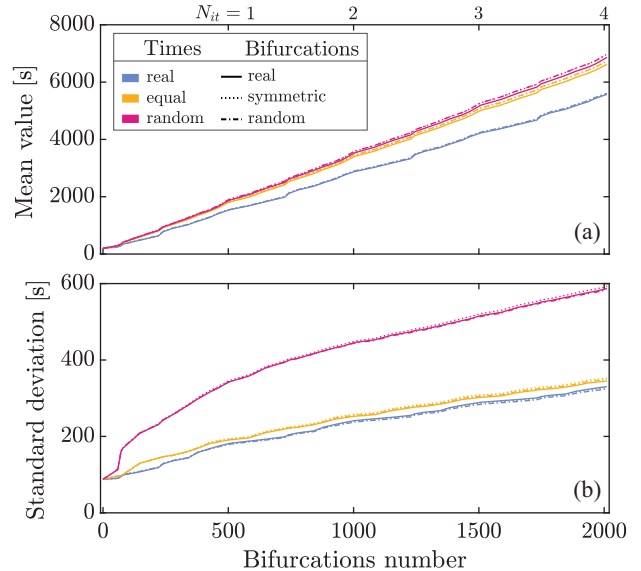


FIG. 8. Mean value and standard deviation over bifurcations number for all nine cases. Labels along the upper  $x$  axis indicate the exit of each network iteration in correspondence with its number of bifurcations. Different colors represent various choices for the edges mean time parameter, while the line styles indicate the type of bifurcation used, as reported in the legend. Lines with the same color tend to overlap due to the dominant role of the choice for mean travel times in the process.

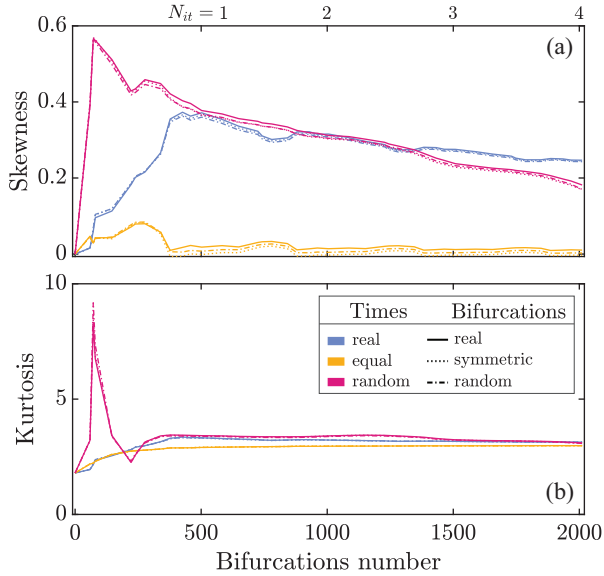


FIG. 9. Skewness and kurtosis over bifurcations number for all nine cases. Labels along the upper  $x$  axis indicate the exit of each network iteration in correspondence with its number of bifurcations. Different colors represent various choices for the edges mean time parameter, while the line styles indicate the type of bifurcation used, as reported in the legend. Lines with the same color tend to overlap due to the dominant role of the choice for mean travel times in the process.

with our observations about Fig. 6, this means that in the cases with realistic travel times the substance reaches the outlet earlier than in the other cases, most likely because of the spatial distribution of the edges. Figure 8(b) displays the evolution of standard deviation. The dispersive character of the process is confirmed, as standard deviation always increases during transport. In particular, the cases with random mean travel times exhibit larger deviations from the mean.

In Fig. 9(a) we observe skewness values of the discharge curves. Skewness starts at zero for all cases, because the input function is symmetric. By looking at the yellow lines, which tend to stay close to zero, we find that the choice of all equal edge travel times corresponds to more symmetric outlet discharge curves, this is again in agreement with the Central Limit Theorem. For the other cases (realistic and random mean travel times), after an initial increase, there is a tendency to decrease towards zero.

For all nine cases, kurtosis in Fig. 9(b) appears to converge, as the number of bifurcations increases, to a value close to 3, which we recall is the kurtosis of a Gaussian distribution. This result expresses correspondence with the plot of Fig. 7, saying that after encountering more bifurcations signals become closer to Gaussians. For the cases with random mean travel times both skewness and kurtosis display a sudden peak at the beginning of the process, which must be attributed to the specific arrangement of the initial edges.

### C. Spatial distribution

Additionally, we give here an analysis of the process from a spatial point of view. We indicate the longitudinal direction of the network by  $x$ , oriented according to the direction of the

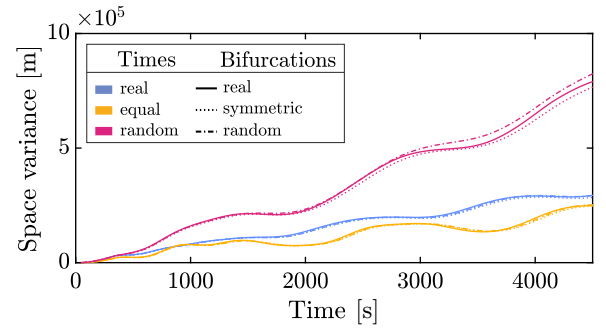


FIG. 10. Temporal evolution of the spatial variance for all nine cases. Different colors represent various choices for the edges mean time parameter, while the line styles indicate the type of bifurcation used, as reported in the legend.

water flow. At every time step  $t$ , let us define the spatial mean and variance weighted over substance flow, respectively, as

$$M_x(t) = \frac{\sum_{i=1}^N x_i Q_{s,i}(t)}{\sum_{i=1}^N Q_{s,i}(t)} \quad \text{and} \quad V_x(t) = \frac{\sum_{i=1}^N [x_i - M_x(t)]^2 Q_{s,i}(t)}{\sum_{i=1}^N Q_{s,i}(t)}, \quad (13)$$

where subscript  $x$  underlines the spatial nature of these variables,  $i = 1, \dots, N$  indicates network edges, and  $x_i$  marks the longitudinal coordinate for the midpoint of edge  $i$ . At  $t = 0$  the substance volume is injected in the inlets, whose longitudinal coordinate correspond to  $x = 0$ . While moving downstream, the substance volume spreads out unevenly in the network due to the presence of several distinct paths. At each time  $t$ , the value of  $M_x(t)$  roughly indicates where the substance volume is (longitudinally) located, while  $V_x(t)$  expresses its longitudinal spread.

In Fig. 10 we show the temporal evolution of the spatial variance  $V_x(t)$  in all nine cases. We mention that the time axis is truncated at  $t = 4500$  because approximately at this moment the substance reaches the end of the compound network for the first time, with  $N_{it} = 4$ . At the beginning of the process, all the substance is concentrated in the inlets; therefore the space variance is close to zero. As time grows, downstream transport causes the substance to spread everywhere in the network; this coincides with a monotonically increasing behavior of the variance. Furthermore, we observe that the highest values of the variance are reached in the cases where times are chosen randomly, while realistic travel times correspond to lower variance values. This might be again linked with the spatial distribution of the  $\lambda_i$ . In the realistic cases, parallel paths have similar travel times, which makes the substance volume travel all together without spreading too much. Apart from some oscillations, which we can trace back to the reinsertion of the signal into the network, the temporal trends of  $V_x$  resemble a linear behavior, typical of Fickian processes [5].

## IV. DISCUSSION

### A. Extension to decaying signals

So far, we have assumed for transported signals to be conservative; however the model presented above can be

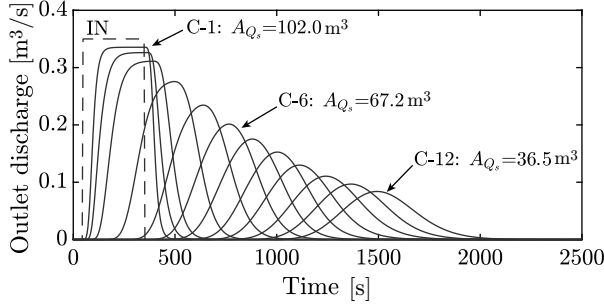


FIG. 11. Outlet discharges for the realistic network case, including exponential decay in the process. The square input function curve is dashed and labeled “IN”. Each of the other curves represents the outlet discharge at a cross section C- $i$ , in order. For clarity, only the labels for cross sections C-1, C-6, and C-12 are indicated, together with the area underlying each curve, corresponding to the volume of substance present in the network.

extended to include signals with temporal decay, as explained in this section. Temporal decay is relevant, for example, for the transport of chemicals whose concentration decreases over time due to reactions (e.g., pollutants in a river or drugs in a biological system). In practice, model extension involves a redefinition of the probability density function  $h(t)$  of Eq. (7). Recalling that  $h(t)dt$  indicates the probability that the particle reaches the outlet in the time interval  $[t, t + dt]$ , this probability is damped as  $t$  grows by a factor we will call  $f_{\text{dec}}(t)$ . The damped probability  $h_{\text{dec}}(t)$  is then found by

$$h_{\text{dec}}(t) = h(t) f_{\text{dec}}(t). \quad (14)$$

Similar to Eq. (8), to account for decay in the computation of network response  $u_{\text{dec}}$  to any input function  $i_0(t)$ , we write

$$u_{\text{dec}}(t) = \int_0^t h(t - \tau) f_{\text{dec}}(t - \tau) i_0(\tau) d\tau. \quad (15)$$

We consider, for instance, the classical first-order exponential decay, so that  $f_{\text{dec}}(t) = e^{-Kt}$ , where  $K$  is the exponential decay constant. Then the network response  $u_{\text{dec}}(t)$  is given by

$$u_{\text{dec}}(t) = \int_0^t h(t - \tau) e^{-K(t-\tau)} i_0(\tau) d\tau. \quad (16)$$

As an example, we perform again a simulation on the Borbera network, using realistic travel time and bifurcation parameters. The decay constant is set to  $K = 2/t_{\text{max}}$  (with  $t_{\text{max}} = 2500$ ) to observe a decay of the injected volume to approximately 30% of the initial value when  $t/t_{\text{max}} \approx 0.6$ . We recall that the substance volume flowing through the network is obtained computing  $A_{Q_i}$ , the area subtended by substance discharge distributions. This value is used to monitor substance decay, as reported in the legend of Fig. 11. As expected, by looking at the substance discharge corresponding to C-12, which peaks around  $t = 1500$  s, we observe a decrease in the substance volume to 30% of the initial value. Conversely, in Fig. 4, where there was no decay, all curves had the same underlying area. Moreover, we notice that even though peaks take place at the same time, their height is different because of the decay. Finally, we still observe the strong dispersive effect caused by the network in the width of the curves.

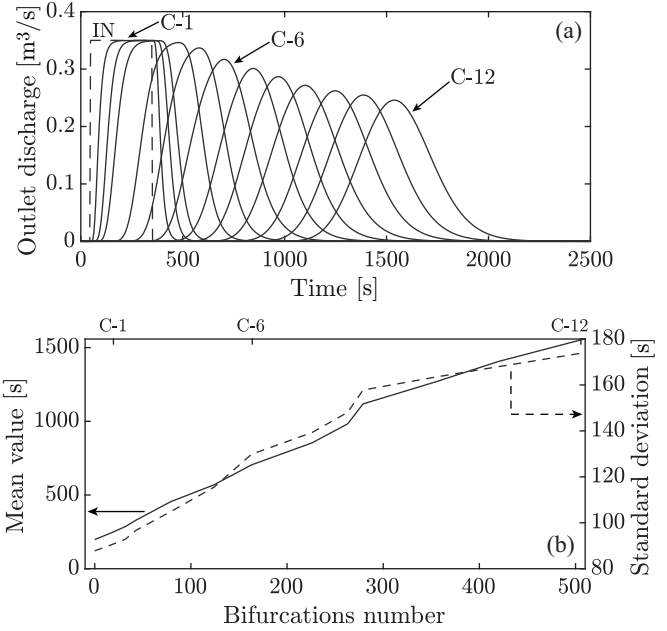


FIG. 12. Results obtained for the reverse network case. In panel (a) the square input function curve is dashed and labeled “IN”. Each of the other curves represents the outlet discharge at a cross section C- $i$ , in order. For clarity, only the labels for cross sections C-1, C-6, and C-12 are indicated. One has to remark the strong similarity to Fig. 4, where the correctly oriented network was used. Panel (b) displays mean value (solid line) and standard deviation (dashed line) of the temporal behavior of the substance outlet discharges plotted over bifurcations number. Continuous and dashed arrows indicate the corresponding y axes.

## B. Model application to other network topologies

In Sec. III, the examples of substance transport through a braided river have shown that signal traveling through a network results in dispersion of the input temporal distribution, and that this depends on edges travel times more than on bifurcation parameters. Additionally, we have observed that in our example the resulting output signal seems to assume a Gaussian-like shape. We now discuss simulations conducted with different networks, in order to speculate on these results and provide a broader view of the model potential, abstracting from the fluvial application.

We first consider a network obtained by flipping the direction of all edges in the Borbera network, that is the reverse of the network in Fig. 3. We remark that, when reversing the network, the number of bifurcations changes by a factor equal to the difference between the number of inlets and outlets in the original network, which in our case is 10. Results, obtained using again realistic parameters, are presented in Fig. 12(a). By comparison with Fig. 4, one can observe a very similar behavior of the outlet discharges along the network. This is confirmed by the metrics shown in Fig. 12(b). Mean value and standard deviation exhibit the same trend and reach the same values as in the realistic case [see Fig. 5(a)]. In particular for the standard deviation, this tells us that encountering a similar number of bifurcations has the same dispersive effect on the process, regardless of the edges disposition. Skewness and kurtosis (not shown for the sake of space), peak earlier with

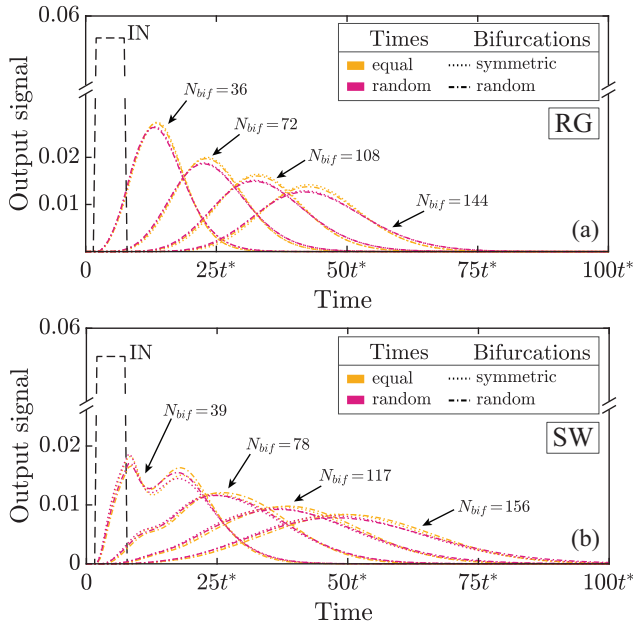


FIG. 13. Output signals for (a) a random graph (RG) and (b) a small-world network (SW). The square input signal is dashed and labeled “IN”. Each of the other curves represents the output signal after passing through the network one to four times, within the plot we indicate the number of bifurcations  $N_{\text{bif}}$  the signal has encountered before reaching the exit. Different colors represent the choices for the edges mean time parameter, while the line styles indicate the type of bifurcation used, as reported in the legend. On the  $x$  axis time is expressed as a multiple of  $t^*$ , i.e., the mean travel time value assigned to all edges in the all-equal case. Note the break on the  $y$  axis.

respect to the process and, then, decrease, stabilizing on the same values of the realistic case [Fig. 5(b)].

To include more general network topologies, we present the results of simulations performed on two canonical network classes: random and small-world networks. As they do not refer to any specific application, we assign parameters arbitrarily. Mean edge travel times are chosen either all equal to a value  $t^*$  or randomly extracted from a gamma distribution with mean  $t^*$ . As for the rules at bifurcations, the signal is either divided either equally among the outgoing edges (we refer to this as “symmetric bifurcation”), or according to values extracted randomly from a uniform distribution between 0.1 and 0.9. While in a river network only bifurcations are present, in other cases splitting at a node may also involve more than two edges (for sake of simplicity in this paragraph we use the word “bifurcation” to indicate a splitting into any number of edges).

The random graph (RG) is composed of 50 nodes and 124 edges and exhibits 36 bifurcations. The small-world network (SW) has 50 nodes, 110 edges, and 39 bifurcations. In both cases, we first generated network topology and then imposed edges orientation, so that no loops are present and that there are exactly one inlet and one outlet. Results are shown in Fig. 13. Notice that the  $y$  axis presents a break for better visualization and that, since travel times are arbitrarily chosen, the  $x$  axis displays time as a multiple of  $t^*$  (the average edge travel time). For each network we input a square function with

underlying area 1 and observe the output signal after one to four network iterations, within the plot we indicate the number of bifurcations encountered by the signal after each passage through the network. We notice that in both Figs. 13(a) and 13(b) the output curves for each network iteration are well overlapped. We can state again that the mean time for the signal to pass through the entire network is the same if we choose all-equal or random edge travel times. Furthermore, in both figures we observe a smoothing and widening of the signal along with the larger number of bifurcations. Figure 13(a) refers to the RG case. Here one observes a good “gaussianization” of the signal even after just the first network iteration. As for Fig. 13(b), it is interesting to notice that, due to the specific SW topology, the first network iteration (corresponding to  $N_{\text{bif}} = 39$ ) results in an output curve with two peaks. This behavior can be ascribed to the high clustering coefficients, typical of small-world networks, which cause less homogeneity among the travel times of different paths. Nevertheless, more passages through the network are able to smooth even these peaks and give the signal a Gaussian-like shape.

## V. CONCLUSIONS

We presented a mathematical framework to formalize the process of network-induced dispersion during signal transport. The resulting model provides a closed-form solution for computing the time distribution of the signal at the outlet based on (i) the network topology, (ii) travel times in the edges, and (iii) splitting rules of the signal at bifurcations. In addition, the model has been extended to include a method for integrating time-dependent decay processes.

We have provided meaningful applications of our modeling, aimed at pointing out the role of each of the three model component. Our results suggest that, fixing the network connectivity structure, edges’ travel times have a more significant impact than bifurcation path probabilities in determining the temporal behavior of discharges at the outlets. Furthermore, we have observed a “gaussianization” in the output signal distributions, which intensifies as the signal passes through more bifurcations.

When dealing with transport processes on networks, it is then important to always consider a dispersive contribution. As we have shown, this is induced by the network itself, regardless of the nature of the phenomenon. Indeed, our methodology is not tied to any specific application but addresses a rather general problem.

Once again our findings confirm the importance of network representation to frame environmental, biological, and social processes in a common mathematical setting.

## ACKNOWLEDGMENTS

This study was carried out within the “e-Capture” project – funded by the European Union – Next Generation EU within the PRIN 2022 program (D.D. 104 - 02/02/2022 Ministero dell’Università e della Ricerca) CUP E53D23004070006. Funded by the European Union (project Grant Agreement No. 101185000 – CONCERTO – HORIZON-CL5-2024-D1-01).

Views and opinions expressed are however those of the author(s) only and do not necessarily reflect those of the European Union or the European Climate, Infrastructure and

Environment Executive Agency (CINEA). Neither the European Union nor the granting authority can be held responsible for them.

**DATA AVAILABILITY**

The data that support the findings of this article are not publicly available. The data are available from the corresponding author upon reasonable request.

**APPENDIX: HYDRAULIC MODELING**

In this appendix we summarize the simplified set of equations used to determine how water flow is distributed at bifurcations, from which we derive the bifurcation probability values for the example. For the sake of simplicity, we refer to an exemplary bifurcation composed of three edges labeled with 0, 1, and 2, with edge 0 splitting into 1 and 2.

For each branch  $i = 0, 1, 2$  let the width  $W_i$ , the water depth  $H_i$  and the specific head  $E_i$  be defined in terms of the water flow  $Q_{w_i}$ , by using hydromorphological relationships proposed by [15]

$$\begin{aligned} W_i(Q_{w_i}) &= 2.36 Q_{w_i}^{0.978} \approx 2.36 Q_{w_i}, \\ H_i(Q_{w_i}) &= K_i(Q_{w_i}) Q_{w_i}^{3/5}, \\ E_i(Q_{w_i}) &= H_i(Q_{w_i}) + \frac{Q_{w_i}^2}{2g W_i(Q_{w_i})^2 H_i^2(Q_{w_i})}. \end{aligned} \quad (A1)$$

Here  $g$  indicates the gravitational constant, while the friction coefficient  $K_i$  depends on sediment diameter  $d$ , slope  $S_i$ , and width  $W_i(Q_{w_i})$  as

$$K_i(Q_{w_i}) = 0.161 d^{1/10} S_i^{-3/10} W_i^{-3/5}.$$

Then, once the flow  $Q_{w_0}$  in branch 0 is known, the unknowns  $Q_{w_1}$  and  $Q_{w_2}$  downstream the bifurcation can be computed by imposing the conservation of flow and specific head at the bifurcation, namely,

$$\begin{aligned} Q_{w_0} &= Q_{w_1} + Q_{w_2}, \\ E_1(Q_{w_1}) &= E_2(Q_{w_2}). \end{aligned} \quad (A2)$$

In the inlet edges water flow is imposed equal to  $35 \text{ m}^3/\text{s}$  divided by the number of inlets, then we are able to compute  $Q_w$  in all downstream branches, by solving system (A2) at every bifurcation. Finally for each channel we derive mean flow velocity  $V_i$  and inverse mean travel time  $\lambda_i$ , using the water flow rate  $Q_{w_i}$ , which we computed, and the edge length  $L_i$ , which is known from network geometry:

$$V_i = \frac{Q_{w_i}}{W_i H_i}, \quad \lambda_i = \left( \frac{L_i}{V_i} \right)^{-1}. \quad (A3)$$

---

[1] M. Newman, *Networks* (Oxford University Press, Oxford, 2018).

[2] S. Boccaletti, V. Latora, Y. Moreno, M. Chavez, and D.-U. Hwang, Complex networks: Structure and dynamics, *Phys. Rep.* **424**, 175 (2006).

[3] P. Ji, J. Ye, Y. Mu, W. Lin, Y. Tian, C. Hens, M. Perc, Y. Tang, J. Sun, and J. Kurths, Signal propagation in complex networks, *Phys. Rep.* **1017**, 1 (2023).

[4] F. Menczer, S. Fortunato, and C. Davis, *A First Course in Network Science* (Cambridge University Press, Cambridge, 2020).

[5] R. B. Bird, W. E. Stewart, and E. N. Lightfoot, *Transport Phenomena* (Wiley, New York, 2006).

[6] I. Rodriguez-Iturbe and J. B. Valdés, The geomorphologic structure of hydrologic response, *Water Resour. Res.* **15**, 1409 (1979).

[7] V. K. Gupta, E. Waymire, and C. T. Wang, A representation of an instantaneous unit hydrograph from geomorphology, *Water Resour. Res.* **16**, 855 (1980).

[8] A. Rinaldo, A. Marani, and R. Rigon, Geomorphological dispersion, *Water Resour. Res.* **27**, 513 (1991).

[9] A. Rinaldo and I. Rodriguez-Iturbe, Geomorphological theory of the hydrological response, *Hydrol. Proc.* **10**, 803 (1996).

[10] R. A. Howard, *Dynamic Probabilistic Systems, Semi-Markov and Decision Processes* (John Wiley, New York, 1971), Vol. II.

[11] A. Karduni, A. Kermanshah, and S. Derrible, A protocol to convert spatial polyline data to network formats and applications to world urban road networks, *Sci. Data* **3**, 160046 (2016).

[12] S. Asmussen, *Applied Probability and Queues* (Springer, New York, 2003).

[13] L. Breuer and D. Baum, *An Introduction to Queueing Theory and Matrix-Analytic Methods* (Springer, Dordrecht, 2005).

[14] M. J. Wilensky, J. Brown, and B. J. Hazelton, Why and when to expect Gaussian error distributions in epoch of reionization 21-cm power spectrum measurements, *Mon. Not. R. Astron. Soc.* **521**, 5191 (2023).

[15] P. Ashmore and E. Sauks, Prediction of discharge from water surface width in braided river with implication for at-a-station hydraulic geometry, *Water Resour. Res.* **42** (2006).